# Water-Induced Degradation of Polymer Solar Cells Studied by $H_2{}^{18}O$ Labeling

**Kion Norrman, Suren A. Gevorgyan, and Frederik C. Krebs***

Risø National Laboratory for Sustainable Energy, Technical University of Denmark, Frederiksborgvej 399, DK-4000 Roskilde, Denmark

**ABSTRACT** Water-induced degradation of polymer photovoltaics based on the active materials poly(3-hexylthiophene) (P3HT) or poly[2-methoxy-5-(2′-ethylhexyloxy)-1,4-phenylenevinylene] (MEHPPV) was studied. The solar cell devices comprised a bulk heterojunction formed by the active material and [6,6]-phenyl-$C_{61}$-butyric acid methyl ester (PCBM) in a standard device geometry. The use of $H_2{}^{18}O$ in conjunction with time-of-flight secondary ion mass spectrometry enabled mapping of the parts of the device that were induced by water. A comparison was made between the two active materials and between devices that were kept in the dark and devices that had been subjected to illumination under simulated sunlight. Devices that were exposed to ambient humidity were compared to devices exposed to saturated humidity. Finally, a comparison was made between results obtained using $H_2{}^{18}O$ and earlier work involving $^{18}O_2$. Water was found to have behavior similar to but not identical with molecular oxygen.

**KEYWORDS:** polymer solar cells • degradation • failure mechanism • TOF-SIMS • P3HT • MEH-PPV



## INTRODUCTION

The exploitation of polymer materials for converting sunlight into electricity through polymer solar cells (1−6) for direct consumption or later usage through external storage is believed to convey several advantages such as lightweightedness, flexibility, environmental friendliness, a low thermal budget, low cost, and most notably very fast modes of production by printing techniques. The research has focused on low-band-gap materials (7, 8), morphology control (9−11), and stability (12) in order to achieve as good performance as possible. The power conversion efficiency currently reaches ∼5% for single junctions (13, 14) and 6.5% for tandem cells (15). The operational stability has reached thousands of hours under laboratory conditions (16−19) and up to a year under outside conditions (20, 21). Production issues are slowly starting to be addressed, and the production of very large area plastic solar cell modules up to 1000 $cm^2$ has been reported (22−24). Production experiments have shown that it is highly feasible with existing technology to mass produce polymer solar cells at a very low cost. While the operational stability has been addressed, an area that has received very little attention is the mechanisms that cause degradation and thus poor stability. All polymer solar cell devices are to some extent unstable and degrade over time. The archetypical polymer solar cell devices based on poly(*p*-phenylenevinylene) (PPV) materials are notoriously unstable under illumination and/or heating. The polythiophenes are more stable, and the current state-of-the-art polythiophenes employ morphologically stable bulk heterojunctions of regioregular poly(3-hexylthiophene) (P3HT) as the donor material and the soluble fullerene material phenyl-$C_{61}$-butyric acid methyl ester (PCBM) as the acceptor material. Stable device operation for 1000 h has been documented for this system (17). Stable operation for more than 10 000 h has been reported for bilayer heterojunctions between regiorandom poly(3-carboxydithiophene) (P3CT) and Buckminster fullerene ($C_{60}$) (18). One could argue that there has been a lot of progress within the areas of processability, efficiency, and stability and that the most serious obstacle for commercialization is the lack of a material that possesses a sufficient degree of all of these vital properties.

In this paper, the stability issue is addressed through studies of degradation. When organic materials are exposed to sunlight, they are subject to photochemical reactions, i.e., intramolecular, intermolecular, or reactions between the constituents of the device and the atmosphere (i.e., oxygen and/or water). Under illumination of organic materials, degradation is inevitable albeit slower under inert conditions. The materials degrade and, as a consequence, so do in many instances their physical, electrical, and mechanical properties. Photovoltaic devices that rely on the delicate interplay between the electronic structure of the material and the energy levels in external electrodes connecting the functional material in the device to the outside world are highly sensitive to even small degrees of degradation. Light absorption and charge-carrier transport properties take place throughout the bulk of the material and at the interfaces. All the processes that are affected by these reaction products in the bulk and at the interfaces will thus lead to degradation of the device performance. The transfers of charges at electrodes or between domains are interface phenomena that are sensitive to impurities or degradation phenomena. The transport of charges in the bulk is also very sensitive to impurities (25). For an electronic device based on organic materials that rely on both bulk and interface phenomena,

* E-mail: frederik.krebs@risoe.dk.
Received for review September 8, 2008 and accepted October 27, 2008
DOI: 10.1021/am800039w



Published on Web 11/24/2008

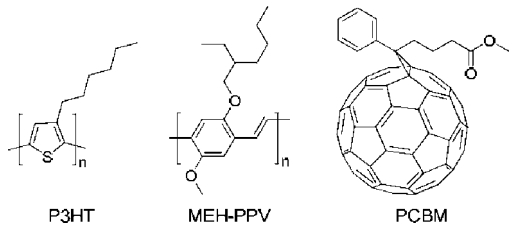


**FIGURE 1. Molecular structures of the active materials used in this study. P3HT: regioregular poly(3-hexylthiophene) (donor material). MEH-PPV: poly[2-methoxy-5-(2′-ethylhexyloxy)-1,4-phenylenevinylene] (donor material). PCBM: phenyl-$C_{61}$-butyric acid methyl ester (acceptor material).**

it is clear that degradation constitutes a serious problem, and must be removed or at least minimized to optimize the lifetime of the device.

Earlier reports from this laboratory focused on the degradation of polymer solar cells induced by molecular oxygen (18, 26−33). By exposure of polymer solar cell devices to dry $^{18}O_2$, it was possible, by use of time-of-flight secondary ion mass spectrometry (TOF-SIMS) (34), to map the degradation processes induced by molecular oxygen during illumination. In this paper, the study is expanded to degradation induced by water, which is carried out by exposure of the polymer solar cell devices to $H_2{}^{18}O$ during illumination and subsequently analysis of the devices using TOF-SIMS methodologies. The study involves a comparative study of water-induced degradation of a bulk heterojunction between P3HT and PCBM and between poly[2-methoxy-5-(2′-ethylhexyloxy)-1,4-phenylenevinylene] (MEH-PPV) and PCBM (Figure 1). The following comparisons are made: (i) a comparison of the two active materials, (ii) a comparison of devices that were kept in the dark and devices that had been subjected to illumination under simulated sunlight, (iii) a comparison of devices that were exposed to ambient humidity and devices that were exposed to saturated humidity, and (iv) a comparison of the result obtained in this study and results obtained in earlier work involving $^{18}O_2$ (18, 26, 28, 31, 32). Detailed knowledge on the degradation mechanisms during illumination and/or storing is vital in the search for finding ways to remove or at least diminish degradation, so that stability will no longer be an issue and an obstacle for the commercialization of polymer solar cells.

## EXPERIMENTAL METHODS

**Photovoltaic Preparation and Characterization.** P3HT and MEH-PPV with weight-average molecular weights ($M_w$) of 35 600 and 65 600 g mol$^{-1}$ and polydispersities (PD) of 1.9 and 4.1 were prepared according to the methods described in the literature (35, 36). Solutions were prepared by dissolving P3HT (25 mg mL$^{-1}$) and PCBM (25 mg mL$^{-1}$) in xylene and MEH-PPV (10 mg mL$^{-1}$) and PCBM (40 mg mL$^{-1}$) in dichlorobenzene followed by microfiltration through a 1 $\mu$m filter. Devices were prepared by spin coating (2800 rpm) an 1.3 wt % aqueous PEDOT:PSS solution onto indium/tin oxide (ITO)-covered glass slides followed by drying at 180 °C for 10 min. The P3HT or MEH-PPV solutions were subsequently spin-coated (800 rpm) onto the PEDOT:PSS layer. Thin (∼100 nm) aluminum electrodes were hereafter evaporated onto the multilayer structure at a pressure of $2 \times 10^{-6}$ mbar, resulting in the following device configuration: Al/X:PCBM/PEDOT:PSS/ITO (X = P3HT or MEH-PPV; Figure 2). The aluminum electrode needs to be thin in order to facilitate peeling of the electrode from the device and to reduce the sputtering time in TOF-SIMS experiments, where depth profiles were obtained by sputtering through the aluminum electrode. The electrode thicknesses were measured using atomic force microscopy (AFM). The final P3HT-based devices were annealed at 150 °C for 5 min. The active areas of the devices were ∼3 cm$^2$. The device geometry has been described earlier (37). The system was purged with argon during removal of the samples for testing. A solar simulator from Steuernagel Lichttechnik GmBH providing AM1.5G illumination conditions was employed for all lifetime measurements under simulated sunlight.

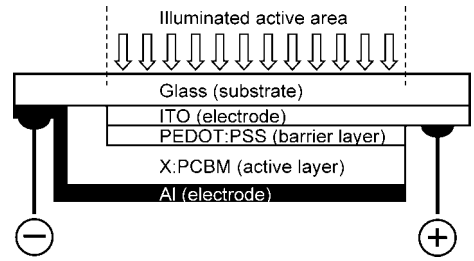


**FIGURE 2. Schematic drawing of the device configuration (Al/X: PCBM/PEDOT:PSS/ITO) used for the two active materials (X = P3HT or MEH-PPV). The active area is ∼3 cm$^2$. The illustration is not drawn to scale.**

The spectral distribution and quality of the solar simulator were monitored using an AvaSpec 2048 spectrometer from Avantes, and a Precision pyranometer from Eppley Laboratories was used to monitor the total power that was set to the desired incident power. The electrical measurements were performed using Keithley 2400 sourcemeters. The photovoltaic performance and stability of the illuminated devices were studied by recording the IV curves at certain times during the experiment.

**$H_2{}^{18}O$ Labeling Studies.** The influence of the atmosphere was established by illumination in a chamber equipped with a quartz window, allowing for control of the atmosphere as described in the literature (37). The freshly prepared solar cells were introduced into the test chamber. $H_2{}^{18}O$ (90%, 5 mL, ∼20 mmol) was then added to the test chamber. The entire system has a volume of 2.5 L, resulting in a saturated isotopically labeled atmosphere. Light was subsequently admitted to half of the devices (the other half were wrapped in aluminum foil), and the short-circuit current ($I_{sc}$) was recorded in order to monitor the device degradation. After 250 h, the devices had degraded and were removed from the chamber and kept in the dark while they were transferrred to the TOF-SIMS analysis chamber. Part of the aluminum electrodes were peeled off by attaching 3M tape to the aluminum electrode followed by removal. This neatly adhered to the aluminum and separated it from the active layer.

**Characterization Using TOF-SIMS Methodologies.** The TOF-SIMS analyses were performed using a TOF-SIMS IV (ION-TOF GmbH, Münster, Germany). TOF-SIMS mass spectra were acquired using 30 ns pulses of 25 keV $Bi_3^+$ that were bunched to form ion packets with a nominal temporal extent of <0.9 ns at a repetition rate of 10 kHz, yielding a target current of 300 fA. These primary ion conditions were used to scan $100 \times 100\ \mu m^2$ areas of the sample surfaces for 30 s corresponding to an ion dose of $6 \times 10^{11}$ ions cm$^{-2}$ (below the static limit). TOF-SIMS images were acquired with equivalent conditions using a lateral resolution of ∼2 $\mu$m over $500 \times 500\ \mu m^2$ areas of the sample surfaces for 393 s corresponding to a ion dose of $7 \times 10^{12}$ ions cm$^{-2}$ (below the static limit). Depth profiling was performed using equivalent conditions with respect to the analysis ions (produced by an analysis gun). For the sputter part of the TOF-SIMS depth profiling, 1.5 kV $Xe^+$ (sputter ions produced by the sputter gun) was used, resulting in a target current of 14 nA. A

**Table 1. Experimental Conditions for the Six Solar Cell Devices That Were Investigated in This Study[a]**

| device no. | active material | relative humidity (%) | temperature (°C) | illumination (W $m^{-2}$) |
|---|---|---|---|---|
| 1 | P3HT | 90 ± 5 | 42 ± 2 | 0 |
| 2 | P3HT | 90 ± 5 | 42 ± 2 | 330 |
| 3 | P3HT | 25 ± 5 | 72 ± 2 | 1000 |
| 4 | MEH-PPV | 90 ± 5 | 42 ± 2 | 0 |
| 5 | MEH-PPV | 90 ± 5 | 42 ± 2 | 330 |
| 6 | MEH-PPV | 25 ± 5 | 72 ± 2 | 1000 |

[a] The content of molecular oxygen ($^{16}O_2$) in the atmosphere was ~20% during all experiments.

**Table 2. Photovoltaic Parameters for Solar Cell Devices That Were Measured in the Ambient Atmosphere Prior to the Degradation Experiment (25 ± 5% Relative Humidity; 72 ± 2 °C) Using AM1.5G Illumination (1000 W $m^{-2}$)[a]**

| active material | $J_{sc}$ (mA $cm^{-2}$) | $V$ (V) | FF | power conversion efficiency (%) |
|---|---|---|---|---|
| MEH-PPV | 3.9 ± 0.03 | 0.83 ± 0.002 | 0.41 ± 0.01 | 1.33 ± 0.02 |
| P3HT | 9.7 ± 0.3 | 0.56 ± 0.002 | 0.31 ± 0.01 | 1.7 ± 0.1 |

[a] Average values are shown with corresponding standard deviations.

400 × 400 $\mu m^2$ area of the surface was sputtered, and the same area (400 × 400 $\mu m^2$) was analyzed. In the subsequent treatment of the data, only the central part was used and possible particles in the material were bypassed in order to exclude nonrepresentative phenomena in the resulting depth profiles. Electron bombardment (20 eV) was used to minimize charge buildup at the surface. Desorbed secondary ions were accelerated to 2 keV, mass analyzed in the flight tube, and postaccelerated to 10 keV before detection.

## RESULTS AND DISCUSSION

Six solar cell devices were constructed: three with an Al/P3HT:PCBM/PEDOT:PSS/ITO configuration and three with an Al/MEH-PPV:PCBM/PEDOT:PSS/ITO configuration. Four of the devices were placed in a chamber with a saturated $H_2{}^{18}O$ atmosphere. The remaining two devices were placed in ambient air. One of each device type (P3HT or MEH-PPV) in the chamber was wrapped loosely in aluminum foil to exclude light but not the atmosphere. The temperatures of the devices in the chamber were similar because of the forced circulation of the atmosphere through a heat exchanger (37). The four devices in the chamber were then exposed to AM1.5G illumination (330 W $m^{-2}$). However, because one of each device type was wrapped in aluminum foil in the chamber, only one of each device type was actually illuminated. The two devices in ambient air were also exposed to AM1.5G illumination (1000 W $m^{-2}$). Table 1 shows what conditions each device was exposed to during the experiment. The degradation of the photovoltaic response was monitored as $I_{sc}$ during illumination, and normalized decay parameters were extracted using a fitting procedure for all illuminated cells.

**IV Characteristics and Degradation.** Table 2 presents the key photovoltaic parameters for solar cell devices that where tested in the ambient atmosphere (25 ± 5% relative humidity; 72 ± 2 °C) using AM1.5G illumination (1000 W $m^{-2}$), and Figure 3 shows the corresponding IV curves measured immediately after device fabrication and prior to stability measurements. Figure 4 shows the short-circuit current−density decay curves for devices measured under different conditions (nos. 2, 3, 5, and 6 in Table 1). The curves in Figure 4 clearly demonstrate a significant impact of humidity on the stability of the solar cells. Devices exposed to ~90% relative humidity and ~42 °C showed significantly faster decay compared to the solar cells exposed

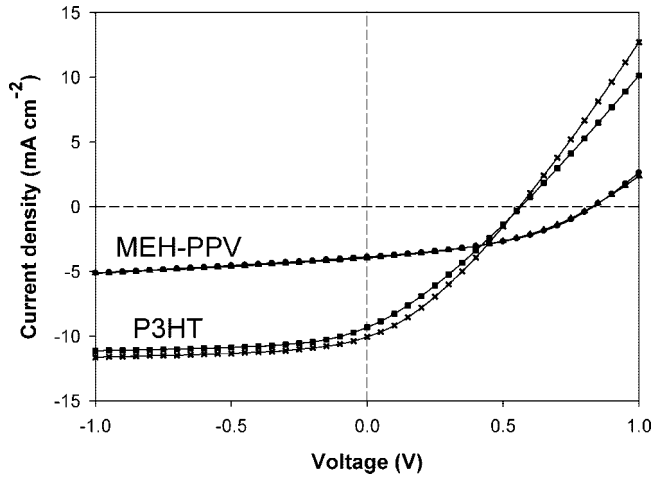


**FIGURE 3. IV curves for solar cell devices that where tested in the ambient atmosphere (25 ± 5% relative humidity; 72 ± 2 °C) using AM1.5G illumination (1000 W $m^{-2}$). Filled squares and crosses correspond to the P3HT:PCBM devices. Filled circles and triangles correspond to the MEH-PPV:PCBM devices.**

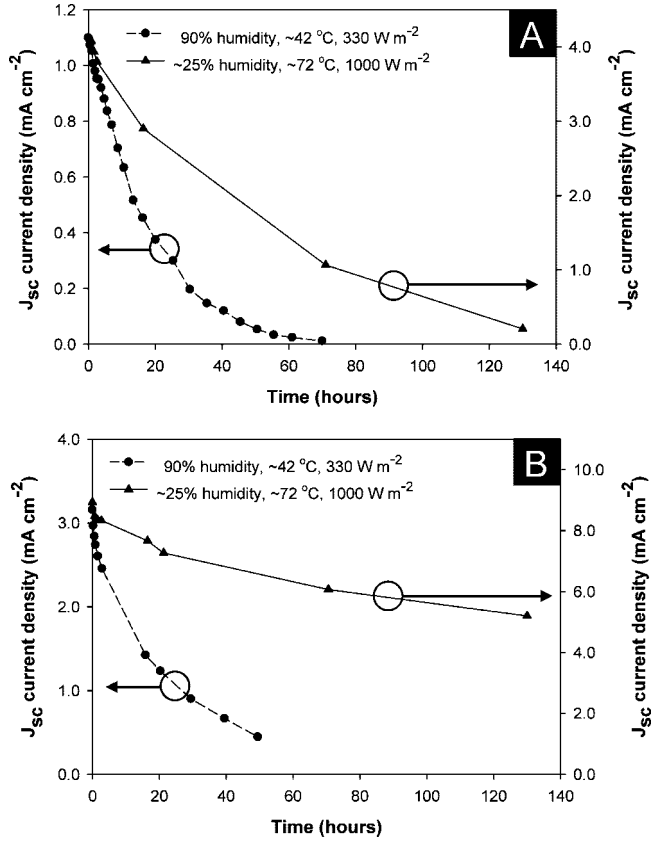


**FIGURE 4. Short-circuit current−density decay curves for the MEH-PPV (A) and P3HT (B) devices.**

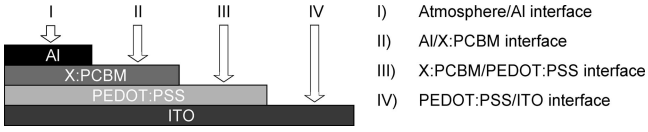


**FIGURE 5. Schematic drawing of a cross-section of a polymer solar cell with the configuration Al/X:PCBM/PEDOT:PSS/ITO showing all the relevant interfaces. X is P3HT or MEH-PPV. The device is not drawn to scale.**

to ~25% relative humidity and ~72 °C in spite of the fact that the samples at ambient humidity were subject to a temperature that is ~30 °C higher and subject to a factor of 3 stronger luminous intensity compared to the conditions of the solar cells in the chamber with ~90% relative humidity. The photovoltaic parameter that changed most was the short-circuit current (see the Supporting Information).

**Characterization Using TOF-SIMS Methodologies.** A polymer solar cell is a multilayer thin film and thus a complex object to analyze. The thin nature (<500 nm) of the device (not considering the substrate) makes it possible to use TOF-SIMS depth profiling to analyze the in-depth (i.e., vertical) and in-plane (i.e., lateral) distribution of chemistry in the device; i.e., three-dimensional information is obtained. However, there are certain problematic phenomena associated with the depth-profiling process that make it wise to consider an additional approach. During the depth-profiling analysis, the surface is bombarded with positively charged sputter ions of such high flux that the charge buildup cannot be adequately compensated for. The consequence is a dramatically reduced sensitivity. Furthermore, the sputter-ion bombardment degrades most of the molecular information, leaving only fragment ions to be analyzed. For example, $C_{60}$ (or PCBM) will only be detected as a series of $C_mH_n^{\pm}$ ions when sputtering is involved but will additionally produce molecular ions ($C_{60}^{\pm}$) when only primary analysis ions are used. Finally, the sputter process causes interlayer mixing, which becomes increasingly worse for longer sputter times. Interlayer mixing makes it difficult (but not impossible) to analyze the interfaces in the multilayer film using depth profiling.

The interfaces in a polymer solar cell could be analyzed using nondestructive techniques such as spectroscopic ellipsometry or X-ray reflectivity (38). However, these provide structural information, and this study focuses primarily on chemical degradation, i.e., water-induced degradation of polymer solar cells, so chemical characterization is preferred such as TOF-SIMS or alternatively X-ray photoelectron spectroscopy. The best additional alternative to analyze the interior of a polymer solar cell with respect to chemistry is thus to systematically remove each layer in the device and analyze the exposed interfaces (II–IV in Figure 5). Only the four polymer solar cell devices that where exposed to isotopically labelled ~90% relative humidity (nos. 1, 2, 4, and 5 in Table 1) were studied using TOF-SIMS methodologies. The solar cell devices were disassembled on only part of the active area, leaving space for depth-profiling analysis through the entire device. The aluminum electrode layer was removed by applying adhesive tape and peeling it off, thus exposing the Al/X:PCBM interface (II in Figure 5) and enabling surface analysis. The X:PCBM layer was removed by gently swabbing a cotton stick soaked in chloroform multiple times across the surface, consequently exposing the X:PCBM/PEDOT:PSS interface (III in Figure 5). The PEDOT:PSS/ITO interface (IV in Figure 5) was exposed in the same way but using a cotton stick soaked in water instead.

All of the interfaces on the four devices were subjected to TOF-SIMS imaging, and a TOF-SIMS depth profile was performed through each device starting from the outer aluminum surface (I in Figure 5) and ending in the glass substrate. The combined results are presented and discussed in the following.

Figure 6 shows depth profiles of the four devices in question starting from the outer aluminum electrode surface (I in Figure 5) and ending somewhere in the active material. It took ~13 h under the given conditions to sputter through the entire device, ending in the glass substrate. However, only the first 1.4 h is informative, so only this part of the depth profiles is shown. Three types of profiles are shown: one for the $AlO_2^-$ intensity (marker for the aluminum electrode, or rather the aluminum oxide part of the aluminum electrode), one for the $C_4^-$ intensity (shared marker for each of the components in the active material X:PCBM), and finally the $^{18}O/^{16}O$ ratio. The $AlO_2^-$ profiles (Figure 6a–d) inform us (not surprisingly) that there is a layer of aluminum oxide on each side of the aluminum electrode. In addition, a logarithmic $AlO_2^-$ intensity scale (Figure 6b) reveals that aluminum oxide is present all the way through the aluminum electrode.

$C_4^-$ is a shared marker for PCBM,P3HT, and MEH-PPV and is observed (as expected) to increase at the Al/X:PCBM interface. The $C_4^-$ profiles have a maximum in the aluminum oxide region. This is due to a matrix effect caused by the vicinity of the oxide. The $AlO_2^-$ and $C_4^-$ profiles are consistent with previous experiments on a similar system using $^{18}O_2$ instead of $H_2{}^{18}O$ (18, 26, 28).

Figure 7 represents an example of how nonideal conditions can be used to extract pseudo depth profiles from a TOF-SIMS ion image. When the sputter-ion beam is rastered over an area, the outcome should ideally be a perfectly box-shaped hole. Instead, the hole is rounded off at the edges, and if the sputtering continues on for a long time, the effect becomes so pronounced that it becomes possible to detect the individual layers in the multilayer device from a subsequent TOF-SIMS imaging analysis over an area that extends the sputter hole. Line profiles can then be extracted from the ion image, e.g., at the dashed white line in Figure 7a, which should qualitatively represent pseudo depth profiles. The depth resolution is, however, even worse than the one obtained from the traditional depth profiling, so this alternative approach has limited applicability. An obvious advantage, however, is an increased sensitivity due to the absence of the parallel sputter process that is a natural part of the depth-profiling procedure. The sputter process incorporates positively charged sputter ions in the surface (i.e., charge buildup) that significantly decreases the signal intensity and thus decreases the sensitivity. After the sputter process and

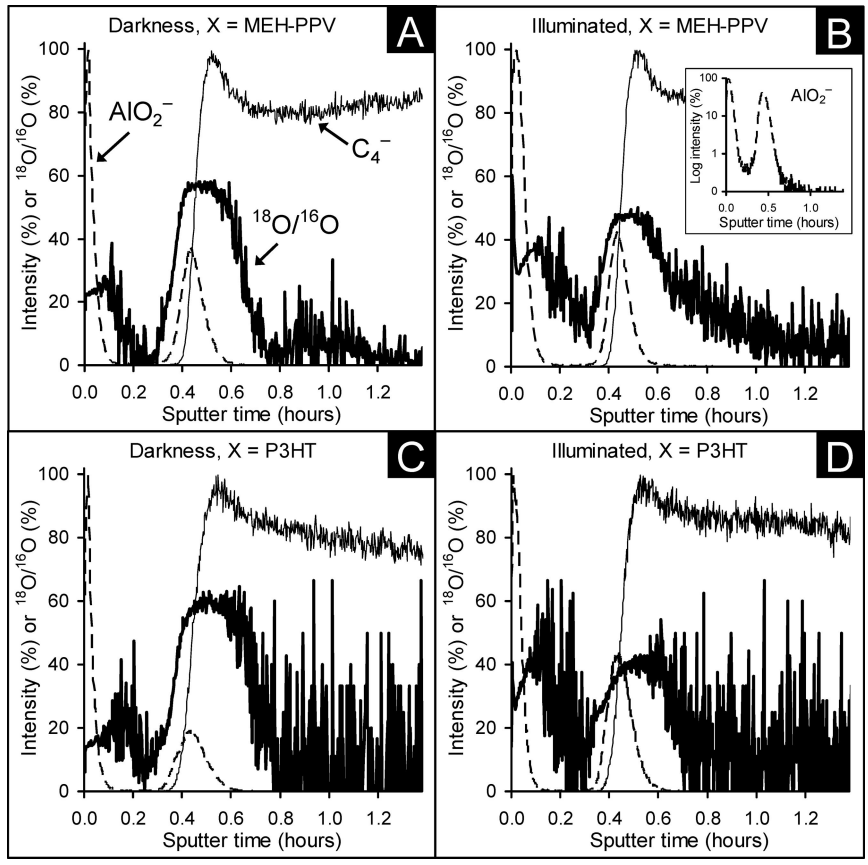


FIGURE 6. TOF-SIMS depth profiles for the devices that were exposed to ~90% relative humidity (nos. 1, 2, 4, and 5 in Table 1). The figures display $^{18}O/^{16}O$ ratios and normalized intensities for selected mass spectral markers as a function of the sputter time. $AlO_2^-$ is a marker for the aluminum electrode, and $C_4^-$ is a marker for the active material X:PCBM (X is P3HT or MEH-PPV). The inset in part B shows the $AlO_2^-$ profile using a logarithmic intensity scale.

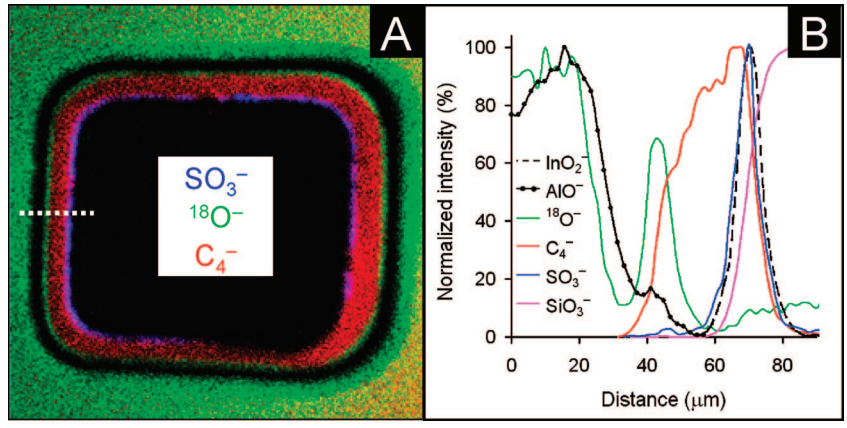


FIGURE 7. (A) TOF-SIMS ion image (500 × 500 $\mu m^2$) covering an entire sputter hole (~400 × 400 $\mu m^2$) after a depth-profiling analysis (Figure 6b) of a device with the configuration Al/P3HT:PCBM/PEDOT:PSS/ITO. $C_4^-$ is a marker for P3HT:PCBM, $SO_3^-$ is a marker for PEDOT:PSS, and $^{18}O^-$ is a marker for $^{18}O$ incorporation or for natural $^{18}O$. (B) Line profiles acquired from the dashed white line in the ion image. $SiO_3^-$ is a marker for the glass substrate, $InO_2^-$ is a marker for ITO, and $AlO^-$ is a marker for the aluminum electrode. The color black in part A is not representative of a particular species; it simply means no intensity.

prior to the imaging analysis, this charge buildup will have had plenty of time to be neutralized.

The $^{18}O/^{16}O$ ratio profiles provide information on the in-depth incorporation of $H_2{}^{18}O$. The natural $^{18}O/^{16}O$ ratio is 0.2%, so if the measured ratio is higher than this value, it must mean that incorporation of water ($H_2{}^{18}O$) occurred during and only during the experiment; i.e., incorporation of $H_2{}^{16}O$ during fabrication and handling is ignored. The marker $^{18}OH^-$ cannot be used because of a mass spectral peak overlap with the intense $F^-$ peak that is always present (contamination). The TOF-SIMS analysis takes place in an ultrahigh vacuum chamber ($10^{-10}$ mbar without a sample and $10^{-8}$–$10^{-9}$ mbar with a sample) so no nonreacted water is present during the analysis; i.e., it is the fixated (reacted) water that is detected.

It is evident from Figure 6a–d that $H_2{}^{18}O$ has been incorporated extensively in the aluminum oxide; i.e., some of the $^{16}O$ atoms have been replaced with $^{18}O$ atoms on the

outer aluminum electrode as well as in the aluminum oxide at the Al/X:PCBM interface. This phenomenon was also observed on a similar system using 1 atm of $N_2/^{18}O_2$ (80:20) for approximately the same period of time (25). However, the only significant difference is the extent of incorporation; in the previous experiment, the detected $^{18}O/^{16}O$ ratio did not exceed ~5% (compared to ~60% in this experiment), which suggests that water is incorporated more efficiently in aluminum oxide compared to molecular oxygen and/or reacts more readily with metallic aluminum. At this point, it can be concluded that water under the given conditions penetrates the aluminum electrode during illumination as well as in darkness. Incorporation of $^{18}O$ into the bulk of the aluminum oxide has presumably no effect on the photovoltaic properties assuming that it is purely a substitutional phenomenon. However, if the oxygen concentration increased in the bulk of the aluminum electrode during the experiment, then the barrier would have increased, which would have affected the photovoltaic properties. No effort was made to clarify whether molecular oxygen (not isotopically labelled) was added to the aluminum electrode during the experiment. It is far more interesting to learn whether $H_2{}^{18}O$ incorporates into the active materials (X:PCBM) at the Al/X:PCBM interface and to see how far into the device $H_2{}^{18}O$ is incorporated.

The right sides of the $^{18}O/^{16}O$ ratio profiles at the Al/X:PCBM interface in Figure 6a–d are rather informative. After ~0.7 h of sputtering (i.e., past the $AlO_2^-$ profile), incorporation presumably occurs in the X:PCBM material. If the $^{18}O/^{16}O$ ratio profile in Figure 6a is compared with the one in Figure 6b, a distinct difference is observed. The $H_2{}^{18}O$ incorporation is clearly more pronounced in MEH-PPV:PCBM for the illuminated device compared to the one that was stored in darkness; i.e., illumination increases the water-induced degradation. This was the same conclusion made in the previous experiments using $^{18}O_2$ (26). For both P3HT devices, the $^{18}O/^{16}O$ ratio profiles are almost nonexistent after ~0.7 h of sputtering because of a significantly high signal-to-noise ratio caused by and an extremely low intensity of $^{18}O^-$. It is now possible to conclude that $H_2{}^{18}O$ degrades MEH-PPV:PCBM in darkness and during illumination in particular. Care should be taken when comparing $^{18}O/^{16}O$ ratios between devices with different configurations. One should consider the "natural" $^{16}O$ content of the materials. For example, P3HT contains no oxygen but MEH-PPV contains two oxygens per monomer unit (Figure 1). However, in this case, the $^{16}O$ contribution will only have dampened the effect observed for MEH-PPV in Figure 6a,b; i.e., the conclusions are still valid.

In summary, from the depth-profiling analysis, it was possible to extract information that shows that water diffuses into the device through the aluminum electrode regardless of whether it is illuminated or not. The depth profiles suggest that water is incorporated more efficiently in aluminum oxide compared to molecular oxygen. Water incorporation is observed to be more pronounced in the MEH-PPV:PCBM layer for the illuminated device compared to the one that was stored in darkness; i.e., illumination increases the water-induced degradation, consistent with earlier observations using $^{18}O_2$ (26).

**Table 3. TOF-SIMS $^{18}O/^{16}O$ Ratios (in %) Measured on the Outer Aluminum Electrode and in Each of the Interfaces for Polymer Solar Cells with the Configuration Al/X:PCBM/PEDOT:PSS/ITO (X = P3HT or MEH-PPV)[a]**

| condition | position analyzed[b] | X = P3HT[c] (%) | X = MEH-PPV[c] (%) |
|---|---|---|---|
| darkness | I | 26.4 ± 0.6 | 26.2 ± 2.6 |
| illuminated | I | 27.4 ± 0.3 | 24.1 ± 1.2 |
| darkness | II | 3.9 ± 0.3 | 11.1 ± 0.3 |
| illuminated | II | 5.6 ± 0.9 | 24.0 ± 0.8 |
| darkness | III | 2.3 ± 0.5 | 4.0 ± 0.1 |
| illuminated | III | 3.6 ± 0.3 | 3.6 ± 0.2 |
| darkness | IV | 4.1 ± 0.4 | 4.3 ± 0.1 |
| illuminated | IV | 3.5 ± 0.1 | 4.5 ± 0.3 |

[a] Each $^{18}O/^{16}O$ ratio is an average of five measurements on different surface locations. [b] The positions refer to Figure 5. [c] X refers to Figure 2 or 5.

On the basis of the signal-to-noise ratios observed in Figure 6a–d at 1.3 h of sputtering, it is tempting to conclude that $H_2{}^{18}O$ incorporation does no exude much further into the device. This is, however, far from the truth; the noisy $^{18}O/^{16}O$ ratio profiles are a consequence of the poor sensitivity caused by the sputter process. TOF-SIMS mass spectra were thus acquired on the outer aluminum electrode surface (I in Figure 5) and in each of the exposed interfaces (II–IV in Figure 5) in order to ascertain how far into the device $H_2{}^{18}O$ incorporation occurs under the given circumstances. Table 3 lists the $^{18}O/^{16}O$ ratios extracted from the TOF-SIMS mass spectra. The values from the outer aluminum electrode (I in Figure 5) should, in principle, be the same but are observed to differ slightly. The errors indicated are standard deviations based on five measurements on different surface locations. However, these are not necessarily representative for the possible sample-to-sample variation. Furthermore, the values in Table 3 for the outer aluminum electrode should not be compared with the values indicated in the $^{18}O/^{16}O$ ratio profiles in Figure 6. There are no zero values in the profiles because the depth-profiling process (unfortunately) begins with the sputter step instead of the analysis step.

When the $^{18}O/^{16}O$ ratios between the P3HT and MEH-PPV devices in the Al/X:PCBM interface (II in Figure 5) are compared, there are convincing differences. $H_2{}^{18}O$ reacts much more efficiently with MEH-PPV:PCBM compared to P3HT:PCBM. If the corresponding ratios for the illuminated devices are compared with the ones stored in darkness, it becomes clear that illumination enhances the $H_2{}^{18}O$ degradation. These observations are consistent with the conclusions made from Figure 6. It is now possible to set up a relative order of water stability for the four devices (or donor/acceptor materials) in question: P3HT:PCBM (darkness) > P3HT:PCBM (illuminated) > MEH-PPV:PCBM (darkness) > MEH-PPV:PCBM (illuminated).

At the X:PCBM/PEDOT:PSS interface (III in Figure 5), there are (as expected) no significant differences except for

a discrepancy between the two devices stored in darkness. The values differ significantly ($2.3 \pm 0.5$ versus $4.0 \pm 0.1$). A possible explanation could be due to insufficient removal of MEH-PPV:PCBM at the interface.

At the PEDOT:PSS/ITO interface (IV in Figure 5), $H_2{}^{18}O$ incorporation is evident; i.e.; $H_2{}^{18}O$ has in all cases penetrated through the entire device to the ITO layer. There are no significant differences in $^{18}O/^{16}O$ ratios between the devices, which suggests either that diffusion through the X:PCBM layer is the same and/or that an equilibrium has had time to be established during the experiment. In a previous experiment (18) using $^{18}O_2$, incorporation was also observed in the ITO, however, with a factor of 10 lower efficiency. Water is apparently more efficiently incorporated into ITO compared to molecular oxygen. The same conclusion was made earlier in this paper for aluminum oxide. A similar experiment (31, 32) was previously performed on a hybrid solar cell with the configuration Ag/MEH-PPV/$Nb_2O_5$/ITO, where it was shown that $^{18}O$ (from $^{18}O_2$) only incorporates into the outer monolayer of oxygen in $Nb_2O_5$. It was, furthermore, shown that in the absence of oxygen in the atmosphere the oxygen is depleted at the MEH-PPV/$Nb_2O_5$ interface (i.e., the outer oxygen monolayer on the $Nb_2O_5$ surface), causing the photovoltaic properties to degrade until oxygen was added to the atmosphere, whereafter the outer oxide layer was reestablished at the $Nb_2O_5$ surface and the photovoltaic properties were reviewed.

In summary, by comparison of mass spectra from all interfaces of the four devices, it was possible to conclude that water diffuses through all layers in the device all the way to the counter electrode (ITO) and that water reacts much more efficiently with MEH-PPV:PCBM compared to P3HT:PCBM. Previous conclusions on the fact that illumination accelerates water-induced degradation are supported by the mass spectral data from the interfaces. The mass spectral investigation of the interfaces enabled a relative order of water stability to be set up for the four devices (or donor/acceptor materials) in question: P3HT:PCBM (darkness) > P3HT:PCBM (illuminated) > MEH-PPV:PCBM (darkness) > MEH-PPV:PCBM (illuminated).

In order to juxtapose our findings with previous work (18, 26), we examined data for isotopic labeling studies at the Al/$C_{60}$ interface using $^{18}O_2$ under both light and dark conditions. One point of reservation is that the two experiments (18, 26) had a different underlying geometry while the Al/$C_{60}$ interface and the conditions of labeling $^{18}O_2$ were similar to this work. Figure 8 shows TOF-SIMS $^{18}O/^{16}O$ ratio images from this previous work (18, 26). The image in Figure 8a was acquired from an Al/$C_{60}$ interface in a device with the configuration Al/$C_{60}$/P3CT/ITO after having been stored in darkness for 800 h in a $N_2/^{18}O_2$ (80:20) atmosphere after degradation in vacuum. The image in Figure 8b was also acquired from an Al/$C_{60}$ interface that was part of a device with the configuration Al/$C_{60}$/$C_{12}$−PSV/PEDOT:PSS/ITO after having been illuminated for 45 h in a $N_2/^{18}O_2$ (80:20) atmosphere. The circularly oriented incorporation in the lateral plane was shown to be a consequence of microscopic

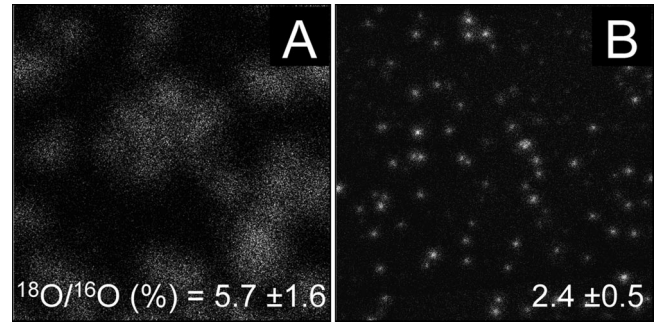


**FIGURE 8. TOF-SIMS $^{18}O/^{16}O$ ratio images (500 × 500 $\mu m^2$) of two different devices: (A) Al/$C_{60}$ interface in a device with the configuration Al/$C_{60}$/P3CT/ITO [P3CT corresponds to poly(3-carboxydithiophene)]; (B) Al/$C_{60}$ interface in a device with the configuration Al/$C_{60}$/$C_{12}$−PSPV/PEDOT:PSS/ITO [$C_{12}$−PSV corresponds to polydidodecylstilbenylenevinylene]. The ratio scale is normalized such that black is zero ratio, gray is some ratio, and white is maximum ratio.**

holes in the aluminum electrode. $^{18}O_2$ diffuses vertically through the holes and expands in all lateral directions, reacting with $C_{60}$, whereafter $^{18}O$ becomes fixated in degradation products. One should bear in mind that the experimental conditions were different (different exposure times, darkness and illumination, and different thicknesses of the aluminum electrode); however, it is still valid to compare the qualitative differences. The spots in Figure 8b are smaller and more intense than the large blurry spots in Figure 8a. The small intense spots suggest that molecular oxygen reacts faster when illuminated. In other words, molecular oxygen reacts in close vicinity to the holes in the lateral plane. In contrast, the device stored in darkness reacts relatively slower and has time to diffuse further in the lateral plane, resulting in bigger but more blurred circular spots. The circular spots were also found in the $C_{12}$−PSV/PEDOT:PSS interface for the Al/$C_{60}$/$C_{12}$−PSV/PEDOT:PSS/ITO device but were not found in the $C_{60}$/P3CT interface for the Al/$C_{60}$/P3CT/ITO device (P3CT was shown to be practically inert toward $^{18}O_2$). However, homogeneous $^{18}O$ incorporation was observed in the ITO surface for both devices, which led to the conclusion that it cannot be ruled out that there is a contribution from the diffusion of $^{18}O_2$ through the grains in the aluminum electrode.

Figure 8 distinguishes incorporation of $^{18}O$ under dark-light conditions for the Al/$C_{60}$ interface using molecular oxygen ($^{18}O_2$) as the source of isotopically labelled oxygen. In contrast, Figure 9 presents TOF-SIMS $^{18}O/^{16}O$ ratio images acquired for the four different experiments carried out here with water ($H_2{}^{18}O$) as the source of isotopically labelled oxygen. The device configuration in this study was Al/X:PCBM/PEDOT:PSS/ITO. The images are obtained in the Al/X:PCBM interface (II in Figure 5). As is evident from all four images, no circular spots are observed except for some slight inhomogeneities. The tiny white dots in Figure 9a,b are mostly normalized noise. These observations suggest that $H_2{}^{18}O$ diffuses efficiently/rapidly through the aluminum grains in the aluminum electrode, causing homogeneous incorporation/degradation. In this case, all electrodes have the same thickness (100 nm). The corresponding images for the remaining interfaces have also practically homogeneous

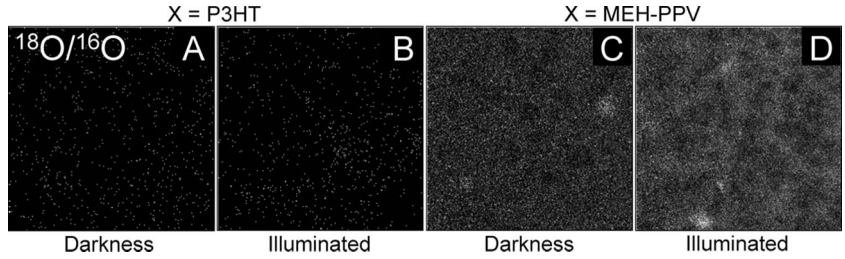


**FIGURE 9. TOF-SIMS $^{18}O/^{16}O$ ratio images (500 × 500 $\mu m^2$) in the Al/X:PCBM interface (II in Figure 5) of the four devices with the configuration Al/X:PCBM/PEDOT:PSS/ITO. X is P3HT or MEH-PPV. The ratio scale is normalized such that black is zero ratio, gray is some ratio, and white is maximum ratio.**

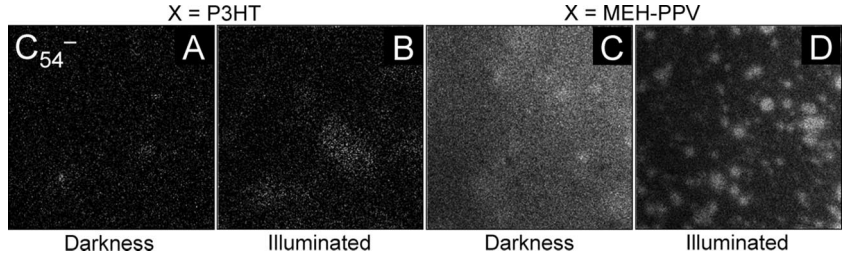


**FIGURE 10. TOF-SIMS ion images (500 × 500 $\mu m^2$) in the Al/X:PCBM interface (II in Figure 5) of the four devices with the configuration Al/X:PCBM/PEDOT:PSS/ITO. X is P3HT or MEH-PPV. $C_{54}^-$ is a marker for degraded PCBM. The intensity scale is normalized such that black is zero intensity, gray is some intensity, and white is maximum intensity.**



$^{18}O/^{16}O$ ratio distributions (not shown). Compared to molecular oxygen, water seems to behave differently with respect to diffusion through the aluminum electrode. However, it could be argued that water could have diffused into the device from the side instead of through the aluminum electrode. This is unlikely because of the extreme ratio between the thicknesses of the various layers (~100 nm) and the width and length of the device (centimeters). The diffusion from the edges is thus expected to be extremely slow (even when the exposure time of 250 h is considered) compared to diffusion through the aluminum electrode.

In summary, the results from an imaging analysis of all interfaces for all four devices suggest that water diffuses efficiently/rapidly through the aluminum electrode between the aluminum grains, causing homogeneous incorporation/degradation in all interfaces. This is a behavior opposite to that of molecular oxygen, which has been shown to at least mainly diffuse through the microscopic pinholes in the aluminum electrode, causing circularly oriented incorporation/degradation, i.e., inhomogeneous incorporation/degradation.

The molecular ion of PCBM (Figure 1) is not sufficiently stable during ionization under the analysis conditions in question; however, the fragment $C_{60}^-$ is (or $C_{60}^+$ for positively charged secondary ions), so $C_{60}^-$ is used as a specific marker for PCBM. If a freshly prepared Al/X:PCBM interface (II in Figure 5) is analyzed, then only $C_{60}^-$ is detected in the high mass region (not shown). The mass spectra for the corresponding interfaces for the exposed (light + heat + $H_2{}^{18}O$ or heat + $H_2{}^{18}O$) devices include peaks corresponding to degraded $C_{60}$; i.e., the $C_{60}$ part of PCBM shows signs of degradation after exposure. These mass spectral peaks correspond mainly to $C_{60-2n}^-$ ($n = 1-4$); i.e., no oxygen-containing ions are detected. The in-plane distribution of one of these fragment ions ($C_{54}^-$) is shown in Figure 10 for the Al/X:PCBM interface for each of the four devices in question. Parts a–c of Figure 10 show fairly homogeneous distributions, but Figure 10d shows a pronounced inhomogeneous $C_{54}^-$ distribution of the same pattern type like the ones shown in Figure 8 for the $^{18}O/^{16}O$ ratio distribution. The $C_{60}^-$ distribution corresponding to Figure 10d is complementary to the $C_{54}^-$ distribution (not shown). From Figure 9, it is fairly certain that $H_2{}^{18}O$ diffuses through the aluminum electrode in a homogeneous manner, i.e., between the aluminum grains. The $C_{54}^-$ distribution in Figure 10d thus suggests that it is the combination of light and molecular oxygen (ambient $^{16}O_2$) that is accelerating the $C_{60}$ degradation. The devices used in this work were exposed to ambient air during fabrication and during transportation to and from equipment. At least molecular oxygen seems to be involved in the degradation mechanism regarding the $C_{60}$ part of PCBM.

The Al/X:PCBM interfaces (II in Figure 5) were additionally analyzed with respect to positive secondary ions. The distribution patterns for $Na^+$ revealed an interesting phenomenon. The P3HT devices have more or less homogeneous distribution patterns, but the MEH-PPV devices have not. In Figure 11c, the sodium is distributed everywhere with an elevated intensity at circular-shaped spots (potassium is concentrated at the dark circular spots). In Figure 11d, the $Na^+$ intensity is even more elevated in the circular spot areas. In addition, the sodium seems to have vanished from the center of the circular spots, leaving rings of sodium. MEH-PPV is probably more hydrophilic after degradation/oxygenation, which would increase the affinity toward $Na^+$ and possibly induce migration of $Na^+$ into the degraded parts of the device. It was not possible to find an explanation as to why $Na^+$ is not present in the center parts of the degraded areas that were presumably degraded by molecular oxygen. There are two possible sodium sources. (i) The obvious one is that it was leftover from the synthesis (i.e., of PCBM, P3HT, or MEH-PPV) because of insufficient purification. (ii) The other source is the PEDOT:PSS layer. PEDOT:PSS typically

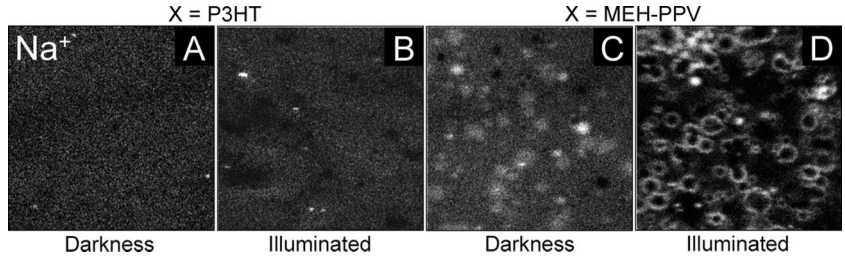


**FIGURE 11. TOF-SIMS ion images (500 × 500 $\mu m^2$) in the Al/X:PCBM interface (II in Figure 5) of the four devices with the configuration Al/X:PCBM/PEDOT:PSS/ITO. X is P3HT or MEH-PPV. The intensity scale is normalized such that black is zero intensity, gray is some intensity, and white is maximum intensity.**

contains a few hundred parts per million of sodium that could have segregated through the active layer to the Al/X:PCBM interface. PEDOT:PSS contains a small excess of PSS that could have acted as a counterion and thus migrated together with $Na^+$. However, PSS was not detected in the interface, which would otherwise have supported the theory that sodium originates from the PEDOT:PSS layer. It is not known what the presence of (or migration of) $Na^+$ has on the photovoltaic properties. The sodium phenomenon is a good example of the fact that an overwhelming amount of (desired and undesired) processes take place during operation of a polymer solar cell. It is impossible to guess how many undesired processes that are still not discovered.

Particle formation in polymer solar cell devices is an area that has received almost no attention. It is thus unknown to what extent particles affect the photovoltaic properties. In previous work from this laboratory, an attempt was made to identify the mechanism for particle formation in an incomplete device (28). The molecular identity of the particles is the key to understanding how the particles are formed. However, to establish the identity of the particles, it is necessary to gain access to them, and that is problematic. The washing procedure used in this work removes the individual layers and thus possible particles located in the bulk of the layers, and possible particles located in the interface will most likely be washed away. Depth profiling is an obvious alternative, but the method suffers from the fact that the sputter process destroys the molecular identity, leaving only small pieces of the puzzle. The particles are visible from the acquired images during a depth-profiling analysis so at least they can be bypassed by software methods as a post-treatment of the data. Possible particle areas were therefore disregarded in the depth profiles presented in Figure 6 in order to avoid nonrelevant complex contributions to the depth profiles.

Possible particles are expected to be formed either in the bulk X:PCBM layer or at the X:PCBM/PEDOT:PSS interface with respect to the devices from this work. In an attempt to image the particles in the device, the following experiment was performed on the illuminated MEH-PPV device starting from the Al/MEH:PCBM interface (II in Figure 5). The images from a depth-profiling analysis were monitored during acquisition. When the images started to show weak signs of particles, the analysis was stopped and the analysis parameters were adjusted to increase the intensity, which caused the acquisition time to increase. To compensate for the increased acquisition time the sputter area size was reduced to ~200 × 200 $\mu m^2$ in order to increase the sputter-ion flux (reduces the depth resolution), which reduced the sputter time and thus the acquisition time. Relevant images are shown in Figure 12 for various relevant sputter time windows. At 5−15 min, particles are detected containing at least sulfur, indium, and silicon. At 15−30 min, particles are indirectly visible as dark spots. The interesting observation is that these particles have a different distribution pattern compared to the ones at 5−15 min. Finally, at 30−45 min, it becomes more or less clear that the second set of particles contains at least carbon, sulfur, and perhaps indium. The observations suggest that PEDOT:PSS and ITO are involved in the particle formation. $C_4^-$ is a shared marker for MEH-PPV, PCBM, and PEDOT:PSS, so it is not possible to conclude whether the active layer is involved or not. One could argue that the observed phenomenon could be due to uneven sputtering; however, such sputter-induced surface/interface irregularities would probably occur on a smaller scale. Care should be taken when interpreting these kinds of images

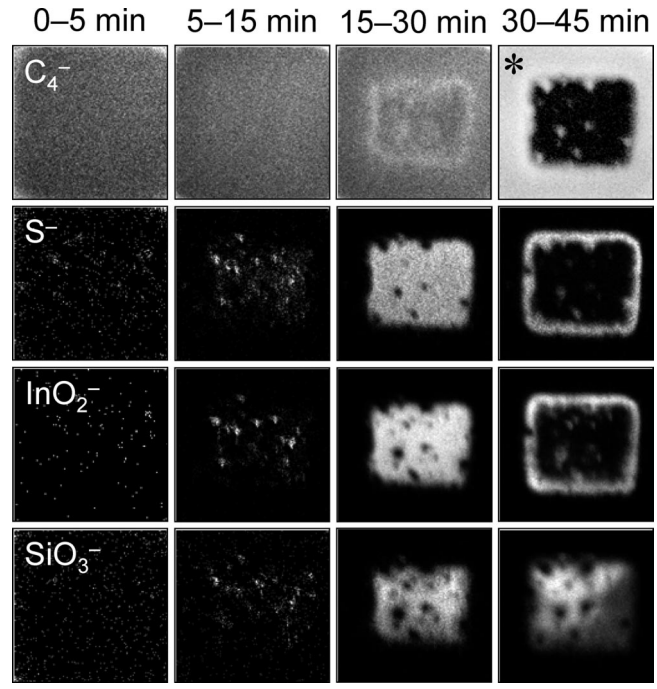


**FIGURE 12. TOF-SIMS ion images (200 × 200 $\mu m^2$) over a sputter hole performed in the Al/MEH-PPV:PCBM interface (II in Figure 5) of a device with the configuration Al/MEH-PPV:PCBM/PEDOT:PSS/ITO that was illuminated. $C_4^-$ is here a shared marker for P3HT, MEH-PPV, and PEDOT:PSS. $S^-$ is a marker for PEDOT:PSS. $InO_2^-$ is a marker for ITO. $SiO_3^-$ is a marker for the glass substrate. The intensity scale is normalized such that black is zero intensity, gray is some intensity, and white is maximum intensity. The image marked with an asterisk has a logarithmic intensity scale.**

(Figure 12). A particle is likely to be eroded (by the sputter process) at a different rate than the surroundings, which would induce uneven sputtering that would continue on. Particle formation in polymer solar cells is rarely commented on in the literature, probably because so little is known about the phenomenon. There is only one example in the literature that describes the phenomenon (28).

In summary, it was possible to extract information from the in-plane and in-depth distribution of some mass spectral markers that were not isotopically labeled. The mass spectral imaging data originating from PCBM suggest that it is the combination of light and molecular oxygen (i.e., not water) that is accelerating the degradation of the $C_{60}$ part of PCBM. The imaging results from the MEH-PPV:PCBM interfaces suggest that sodium possibly segregates to locations with a relatively large extent of degradation (caused by molecular oxygen) possibly because of the higher hydrophilicity. For the illuminated MEH-PPV:PCBM interface, sodium had vanished from the center part of the degraded areas. No explanation was found for this phenomenon. An in-depth analysis of selected nonisotopically labeled mass spectral markers suggests that at least two types of particles are found in at least the illuminated MEH-PPV device. One type of particles contains at least sulfur, indium, and silicon. The other type contains at least carbon, sulfur, and perhaps indium. The observations regarding particles suggest that PEDOT:PSS and ITO are involved in the particle formation. It was not possible to conclude whether the active layer is involved in particle formation or not. It was not possible to conclude anything about to what extent particles influence the photovoltaic properties.

## CONCLUSIONS

Water-induced degradation of polymer solar cells with the configuration Al/X:PCBM/PEDOT:PSS/ITO (X = P3HT or MEH-PPV) was studied. The use of $H_2{}^{18}O$ in conjunction with TOF-SIMS methodologies enabled mapping of the parts of the device that were induced by water. A comparison was made between P3HT:PCBM and MEH-PPV:PCBM and between devices that were kept in the dark and devices that had been subjected to illumination under simulated sunlight. Furthermore, devices that were exposed to ambient humidity were compared to devices exposed to saturated humidity. The current result obtained using $H_2{}^{18}O$ was compared with earlier work involving $^{18}O_2$.

Short-circuit current−density decay curves of solar cell devices that were exposed to a saturated water atmosphere during operation revealed a significant degradation of the stability when compared to the corresponding devices exposed to ambient humidity.

A depth-profiling analysis showed that water diffuses into the device through the aluminum electrode regardless of whether it is illuminated or not. Water appears to be incorporated more efficiently in aluminum oxide compared to molecular oxygen. Water incorporation is observed to be more pronounced in the MEH-PPV:PCBM layer for the illuminated device compared to the one that was stored in darkness; i.e., illumination increases the water-induced degradation, consistent with earlier observations using $^{18}O_2$.

Possible incorporation of $^{18}O$ in the various interfaces was determined from the $^{18}O/^{16}O$ ratio extracted from the mass spectral data. On the basis of these findings, it was possible to conclude that water diffuses through all layers in the device all the way to the counter electrode (ITO). Furthermore, it was found that water reacts much more efficiently with MEH-PPV:PCBM compared to P3HT:PCBM and that illumination accelerates water-induced degradation, consistent with the depth-profiling results. The mass spectral investigation of the interfaces suggests that the relative stability of the donor/acceptor materials in question is P3HT:PCBM (darkness) > P3HT:PCBM (illuminated) > MEH-PPV:PCBM (darkness) > MEH-PPV:PCBM (illuminated).

An imaging analysis of all interfaces for all four devices suggests that water diffuses efficiently/rapidly through the aluminum electrode between the aluminum grains, causing homogeneous incorporation/degradation in all interfaces. This is a behavior opposite to that of molecular oxygen, which has been shown to at least mainly diffuse through the microscopic pinholes in the aluminum electrode, causing circular oriented incorporation/degradation, i.e., inhomogeneous incorporation/degradation.

An imaging analysis based on mass spectral markers that were not isotopically labeled showed that it is the combination of light and molecular oxygen (i.e., not water) that is accelerating the degradation of the $C_{60}$ part of PCBM. The imaging results from the MEH-PPV:PCBM interfaces suggest that sodium possibly segregates to locations with a relatively large extent of degradation (caused by molecular oxygen) possibly because of the higher hydrophilicity. For the illuminated MEH-PPV:PCBM interface, sodium had vanished from the center part of the degraded areas. No explanation was found for this phenomenon. An in-depth imaging analysis of selected nonisotopically labeled mass spectral markers suggests that at least two types of particles are found in at least the illuminated MEH-PPV device. The observations regarding particles suggest that at least PEDOT:PSS and ITO are involved in the particle formation. It was not possible to conclude anything about to what extent particles influence the photovoltaic properties.

**Acknowledgment.** This work was supported by the Danish Strategic Research Council (DSF 2104-04-0030, 2104-05-0052, and 2104-07-0022).

**Supporting Information Available:** Evolution of the IV curves as a function of time/degradation and plots of TOF-SIMS depth profiles showing the level of $^{18}O$ incorporation in the bulk of the aluminum electrode on a logarithmic scale. This material is available free of charge via the Internet at http://pubs.acs.org.

## REFERENCES AND NOTES

(1) Brabec, C. J.; Sariciftci, N. S.; Hummelen, J. C. *Adv. Funct. Mater.* **2001**, *11*, 15–26.
(2) Spanggaard, H.; Krebs, F. C. *Sol. Energy Mater. Sol. Cells* **2004**, *83*, 125–146.

(3) Coakley, K. M.; McGehee, M. D. *Chem. Mater.* **2004**, *16*, 4533–4542.
(4) Hoppe, H.; Sariciftci, N. S. *J. Mater. Res.* **2004**, *19*, 1924–1945.
(5) Günes, S.; Neugebauer, H.; Sariciftci, N. S. *Chem. Rev.* **2007**, *107*, 1324–1338.
(6) Krebs F. C. *Polymer Photovoltaics a Practical Approach*; SPIE Press: Bellingham, WA, 2008.
(7) Winder, C.; Sariciftci, N. S. *J. Mater. Chem.* **2004**, *14*, 1077–1086.
(8) Bundgaard, E.; Krebs, F. C. *Sol. Energy Mater. Sol. Cells* **2007**, *91*, 954–985.
(9) Thompson, B. C.; Fréchet, J. M. J. *Angew. Chem., Int. Ed.* **2008**, *47*, 58–77.
(10) Hoppe, H.; Sariciftci, N. S. *J. Mater. Chem.* **2006**, *16*, 45–61.
(11) Yang, X.; Loos, J. *Macromolecules* **2007**, *40*, 1353–1362.
(12) Jørgensen, M.; Norrman, K.; Krebs, F. C. *Sol. Energy Mater. Sol. Cells* **2008**, *92*, 686–714.
(13) Li, G.; Shrotriya, V.; Huang, J.; Yao, Y.; Moriarty, T.; Emery, K.; Yang, Y. *Nat. Mater.* **2005**, *4*, 864–868.
(14) Ma, W.; Yang, C.; Gong, X.; Lee, K.; Heeger, A. J. *Adv. Funct. Mater.* **2005**, *15*, 1617–1622.
(15) Kim, J. Y.; Lee, K.; Coates, N. E.; Moses, D.; Nguyen, T. Q.; Dante, M.; Heeger, A. J. *Science* **2007**, *317*, 222–225.
(16) Krebs, F. C.; Spanggaard, H. *Chem. Mater.* **2005**, *17*, 5235–5237.
(17) Yang, X.; Loos, J.; Veenstra, S. C.; Verhees, W. J. H.; Wienk, M. M.; Kroon, J. M.; Michels, M. A. J.; Janssen, R. A. J. *Nano Lett.* **2005**, *5*, 579–583.
(18) Krebs, F. C.; Norrman, K. *Prog. Photovoltaics* **2007**, *15*, 697–712.
(19) Bjerring, M.; Nielsen, J. S.; Siu, A.; Nielsen, N. C.; Krebs, F. C. *Sol. Energy Mater. Sol. Cells* **2008**, *92*, 772–784.
(20) Katz, E. A.; Gevorgyan, S.; Orynbayev, M. S.; Krebs, F. C. *Eur. Phys. J. Appl. Phys.* **2007**, *36*, 307–311.
(21) Hauch, J. A.; Schilinsky, P.; Choulis, S. A.; Childers, R.; Biele, M.; Brabec, C. J. *Sol. Energy Mater. Sol. Cells* **2008**, *92*, 727–731.
(22) Krebs, F. C.; Spanggaard, H.; Kjær, T.; Biancardo, M.; Alstrup, J. *Mater. Sci. Eng. B* **2007**, *138*, 106–111.
(23) Krebs, F. C.; Alstrup, J.; Spangaard, H.; Larsen, K.; Kold, E. *Sol. Energy Mater. Sol. Cells* **2004**, *83*, 293–300.
(24) Lungenschmied, C.; Dennler, G.; Neugebauer, H.; Sariciftci, N. S.; Glatthaar, M.; Meyer, T.; Meyer, A. *Sol. Energy Mater. Sol. Cells* **2007**, *91*, 379–384.
(25) Liu, A.; Zhao, S.; Rim, S. B.; Wu, J.; Könemann, M.; Erk, P.; Peumans, P. *Adv. Mater.* **2008**, *20*, 1065–1070.
(26) Norrman, K.; Krebs, F. C. *Sol. Energy Mater. Sol. Cells* **2006**, *90*, 213–227.
(27) Alstrup, J.; Norrman, K.; Jørgensen, M.; Krebs, F. C. *Sol. Energy Mater. Sol. Cells* **2006**, *90*, 2777–2792.
(28) Norrman, K.; Larsen, N. B.; Krebs, F. C. *Sol. Energy Mater. Sol. Cells* **2006**, *90*, 2793–2814.
(29) Norrman, K.; Alstrup, J.; Krebs, F. C. *Surf. Interface Anal.* **2006**, *38*, 1302–1310.
(30) Lira-Cantu, M.; Krebs, F. C. *Sol. Energy Mater. Sol. Cells* **2006**, *90*, 2076–2086.
(31) Lira-Cantu, M.; Norrman, K.; Andreasen, J. W.; Krebs, F. C. *Chem. Mater.* **2006**, *18*, 5684–5690.
(32) Lira-Cantu, M.; Norrman, K.; Andreasen, J. W.; Casan-Pastor, N.; Krebs, F. C. *J. Electrochem. Soc.* **2007**, *154*, B508—B513.
(33) Norrman, K.; Krebs, F. C. *Proc. SPIE* **2005**, *5938*, 59380D.
(34) Vickerman J. C.; Briggs D. *TOF-SIMS Surface Analysis by Mass Spectrometry*; IM Publications and Surface Spectra Ltd.: West Sussex, U.K., 2001.
(35) Neef, C. J.; Ferraris, J. P. *Macromolecules* **2000**, *33*, 2311–2314.
(36) McCullough, R. D.; Lowe, R. D.; Jayaraman, M.; Anderson, D. L. *J. Org. Chem.* **1993**, *58*, 904–912.
(37) Gevorgyan, S. A.; Jørgensen, M.; Krebs, F. C. *Sol. Energy Mater. Sol. Cells* **2008**, *92*, 736–745.
(38) Andreasen, J. W.; Gevorgyan, S. A.; Schlepütz, C. M.; Krebs, F. C. *Sol. Energy Mater. Sol. Cells* **2008**, *92*, 793–798.

AM800039W